atoms

MDPI

Article

High-Resolution Fourier Transform Spectra of Atomic Sulfur: Testing of Modified Quantum Defect Theory

Vladislav E. Chernov [1,*], Nikolai L. Manakov [1], Alexei V. Meremianin [1], Alexander V. Naskidashvili [1], Svatopluk Civiš [2], Martin Ferus [2], Petr Kubelík [2], Ekaterina M. Zanozina [2] and Oxana V. Zetkina [3]

[1] Physics Faculty, Voronezh State University, 394018 Voronezh, Russia
[2] J. Heyrovský Institute of Physical Chemistry, Academy of Sciences of the Czech Republic, Dolejškova 3, 18223 Prague, Czech Republic
[3] Economics and Mathematics Department, P. G. Demidov Yaroslavl' State University, 150003 Yaroslavl', Russia
* Correspondence: chernov@niif.vsu.ru

Abstract: QDT (quantum defect theory) is an effective technique for calculating processes involving highly excited (Rydberg) states of atoms, ions, and molecules with one valence electron outside filled shells, whose spectrum generally resembles a hydrogen-like atom's spectrum. At the expense of some modification of QDT, in this paper, we extend its applicability to describe low- and intermediate-excited levels of atoms with more complex spectra (on the example of atomic sulfur S I). Transitions between just such states are responsible for the infrared (IR) spectra of atoms. While the quantum defects (QDs) of the highly excited Rydberg levels are determined by the energies of *individual* levels near the ionization threshold, the radial wave functions of low excited electronic states, in the framework of our modification of QDT, include the QD dependence on energy over a wide energy range; this dependence is determined from the *whole* spectral series. We show that, outside the atomic core domain, the electron radial functions calculated using modified semi-phenomenological QDT agree well with ab initio calculations. As another assessment of QDT accuracy, we show satisfactory agreement of the probabilities of dipole transitions in S I, taken from the NIST Atomic Spectra Database, with our QDT calculations. We perform an indirect experimental verification of QDT on the basis of spectra of S I in gas-discharge plasma measured by time-resolved high-resolution Fourier transfer spectroscopy (FTS). The Boltzmann plot built from our measured spectra demonstrates that QDT provides a satisfactory approximation for calculating the experimental lines' intensities.

Keywords: atomic spectra; Rydberg states; quantum defect; high-resolution infrared Fourier transform spectroscopy

check for updates

Academic Editor: Jean-Christophe Pain

Received: 7 January 2025
Revised: 1 February 2025
Accepted: 6 February 2025
Published: 8 February 2025

Citation: Chernov, V.E.; Manakov, N.L.; Meremianin, A.V.; Naskidashvili, A.V.; Civiš, S.; Ferus, M.; Kubelík, P.; Zanozina, E.M.; Zetkina, O.V. High-Resolution Fourier Transform Spectra of Atomic Sulfur: Testing of Modified Quantum Defect Theory. *Atoms* **2025**, *13*, 16. https://doi.org/10.3390/atoms13020016

Copyright: © 2025 by the authors. Licensee MDPI, Basel, Switzerland. This article is an open access article distributed under the terms and conditions of the Creative Commons Attribution (CC BY) license (https://creativecommons.org/licenses/by/4.0/).

1. Introduction

One of the fundamental tasks of astrophysics is to determine the detailed chemical composition of as many objects (stars, planets, interstellar clouds) as possible. In recent decades, astronomical observations in the infrared (IR) range have become increasingly important. The instrumental capabilities of infrared astronomy are constantly evolving and now include many observatories—ground, airborne, and space [1].

To meet the growing demands of infrared (IR) astrophysics, we need large amounts of spectroscopic data (such as level energies, line wavenumbers, probabilities of radiative transitions or oscillator strengths [2], electron scattering cross sections [3], atomic collisions [4], photoionization and recombination [5,6], Stark line broadening parameters [7], etc.) for a large number of atoms, including transitions involving excited (Rydberg) levels [8].

It should be noted that ab initio calculations of atomic structures for Rydberg states encounter significant difficulties [9], and the accuracy of the energy level calculations is much lower than the experimental accuracy of their spectroscopic measurement. Therefore, of particular relevance are methods that can combine the possibility of analytical representation of the results (and, therefore, computational simplicity) with the possibility of calculating electron transition matrix elements through experimental energy levels.

QDT (quantum defect theory, [10]) meets the above requirements. QDT assumes that the processes of radiation–atom interaction involve one "optical" Rydberg, which moves at a considerable distance from the atomic (molecular) core. The energies of this electron, E_{nl}, in the core potential form a spectral series similar to those of a hydrogen-like atom; these spectral series are given by the following well-known expression:

$$E_{nl} = E_{\mathrm{IP}} - \frac{Z^2}{2(n-\mu_l)^2} = E_{\mathrm{IP}} - \frac{Z^2}{2\nu_{nl}^2}. \quad (1)$$

According to the Rydberg Formula (1), each Rydberg series of levels with the orbital quantum number l consists of infinitely many levels, numbered by the integer principal quantum number n, that converge (at $n \to \infty$) to the ionization threshold, or ionization potential (IP), E_{IP}. The energies of this level series, E_{nl}, are expressed in terms of quantum defect (QD)—$\mu_l = n - \nu_{nl}$, where ν_{nl} is the effective (non-integer) quantum number ν—and the integer principal quantum number. For neutral atoms, the core charge $Z = 1$.

QDT can be useful for many problems in atomic and plasma physics [11], in particular, for describing processes involving Rydberg states, such as photoionization [12–14], collisions of excited atoms and molecules [15–18] (including those accompanied by the development of dynamic chaos [19]), etc.

The simplicity of Rydberg Formula (1) is due to the main approximation of QDT: the potential of the atomic core can be considered Coulombic at large distances, i.e., $r > r_c$, where r_c is an effective dimension of the core. The shape of the potential in the intra-core domain ($r < r_c$) is unknown, but a whole spectral Rydberg l-series (with high n corresponding to sufficiently highly excited levels) can be determined from *one* quantum defect, μ_l, the latter being computed from *any* (sufficiently high) level energy of the experimental l-series. The quantum defects μ_l play in QDT a role similar to $\{l_{\mathrm{eff}}\}$ values appearing in the method of model potential [20–22]. Here, the curly brackets surround the fractional part, with $\{l_{\mathrm{eff}}\}$ being the effective orbital number, which is not an integer parameter of the model potential technique.

The semi-phenomenonlogical character of QDT (and the model potential method) consists in the fact that the quantum defects μ_l (or, in other words, the effective principal quantum numbers ν_{nl}) are determined from experimental data, and the wave functions of the Rydberg electron in the region $r > r_c$ (outside the ionic core) are calculated analytically. Using these wave functions, one can calculate amplitudes of atom–photon interaction processes. In particular, to calculate multiphoton processes in atoms with one valence electron over closed shells in the QDT approximation, an analog of the Coulomb Green's function (QDT-GF) [23,24] has been constructed. From QDT-GF, the radial electron wave functions can also be calculated. These functions, like the QDT-GF, depend on the quantum defects μ_l, which contain the experimental information about the spectrum of the atom.

As mentioned above, in numerous applications, QDT is used for atoms with a single electron outside the filled shells only. Here, we use wave functions obtained using a modified QDT-GF method to analyze spectra of more complex atoms that have several electrons over the filled shells. As an application, we compute an array of transition probabilities in neutral sulfur atom S I to analyze its high-resolution Fourier spectra in a gas discharge plasma.

Sulfur is a vital element in chemical, biological, and environmental processes, making it a major focus for researchers [25]. It is one of the most abundant elements in the universe, closely following hydrogen, carbon, nitrogen, and oxygen in the solar system. Sulfur lines have been observed in the spectra of the Sun and other astrophysical objects. The abundance and distribution of sulfur provide valuable insights into the chemical evolution of galaxies, stars, and planets. For instance, understanding the distribution of sulfur helps us comprehend the connection between the composition of planets and the formation processes in protoplanetary disks [26]. Sulfur is a crucial element in studies of the atomic composition of planetary nebulas, as it unveils the chemical evolution occurring in specific regions of the galaxy [27].

Let us describe the general outline of this work. Section 3.1 presents explicit formulae for the electron radial wave functions in QDT approximation together with general formulae for dipole transition matrix elements in *LS* coupling. Section 3.2 briefly describes the design of the experiment in which the spectra of sulfur-containing plasma discharge were recorded. Section 2 compares the radial wave functions computed by QDT with those calculated using an ab initio (Hartree–Fock) method. This comparison proves the suitability of QDT for low excited terms of S I, not only for highly excited Rydbergs. We compare the probabilities of transitions involving S I $(^4S)nl$ levels taken from the NIST ASD (Atomic Spectra Database) [28] with those calculated within the QDT framework. From the measured IR spectra of S I, we construct a Boltzmann plot that demonstrates the reasonable accuracy of the QDT calculations of transition probabilities to describe the observed line intensities in discharge plasma spectra.

2. Results and Discussion

The strongest S I spectral lines in the 7000–11,000 cm^{-1} region corresponding to triplet–triplet and quintet–quintet $4s$–$4p$ transitions, as well as quintet–quintet $4p$–$5s$ transitions, are shown in Figure 1.

In Figure 2, we compare two calculations for radial wave functions of some of the above-mentioned terms. Solid lines correspond to QDT calculations (4), and the dots represent ab initio (using Robert D. Cowan's code described in the book [29]; see also [30]). Figure 2 shows quantitative agreement between QDT and ab initio calculations even for lowest levels in s- and p-series over a wide range of the radial variable r except for a small intra-core region, $r \lesssim r_c$. In QDT approximation, the radial wave function $P_{nl}(r)$ has $n_r = \mathrm{Int}(\nu_{nl}) - l - 1$ nodes (Int denotes the nearest integer number) outside the core ($r \gtrsim r_c$). The radial quantum number n_r is assigned in the model potential theory [20–22,31,32] for levels in a nl-series in the order of increasing energy, starting from $n_r = 0$ for the lowest-excited level of each nl-series. The effective principal quantum number, $n_{\mathrm{eff}} = \nu_{nl} = n_r + l_{\mathrm{eff}} + 1$, in the model potential technique is calculated through the so-called effective orbital number $l_{\mathrm{eff}} = \nu_{nl} - n_r - 1$, which is *non-integer*.

QDs μ_l and principal quantum numbers ν_{nl} of some terms of S I (including those indicated in Figures 1 and 2) are presented in Table 1. As one can see from this table, the indicated values of n_r coincide with the number of nodes (outside the core) of the corresponding wave functions shown in Figure 2. Note that some negative l_{eff} appear in Table 1. The radial wave function in the model potential framework has a behavior $P_{nl}(r) \propto r^{1+l_{\mathrm{eff}}}$ at $r \to 0$, so small negative l_{eff} do not influence on the convergence of radial integral at small r. They are given in Table 1 for illustrative purposes only; our calculations do not use model potential wave functions.

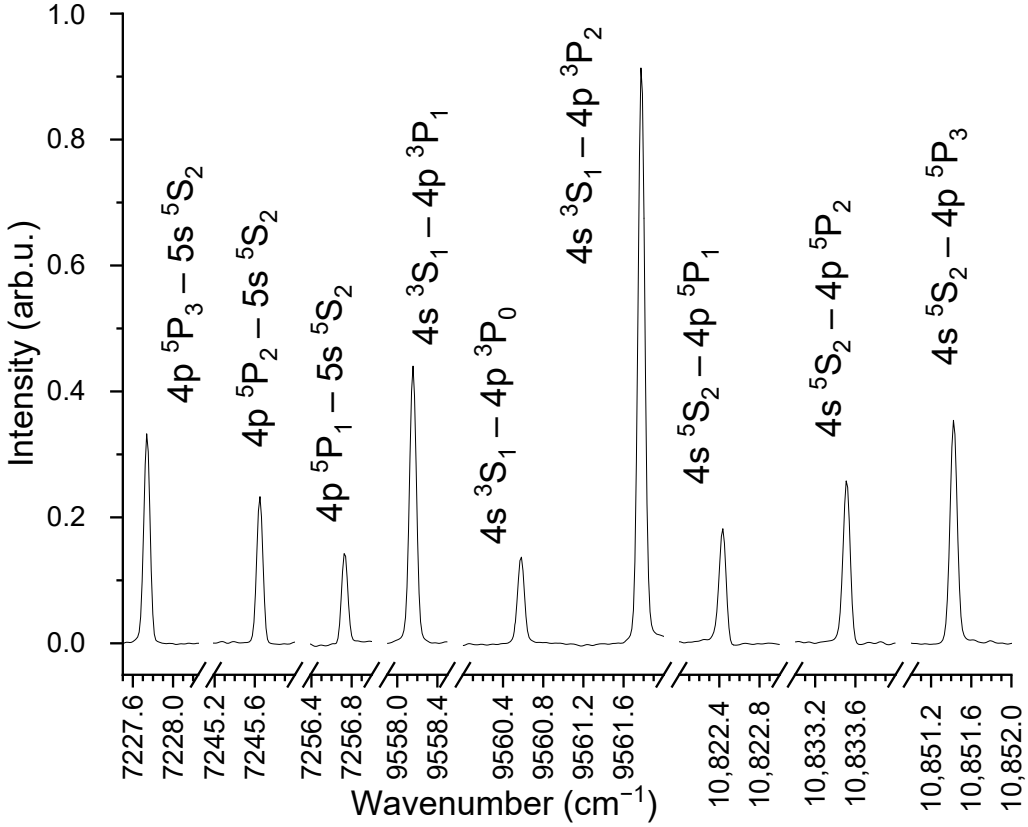
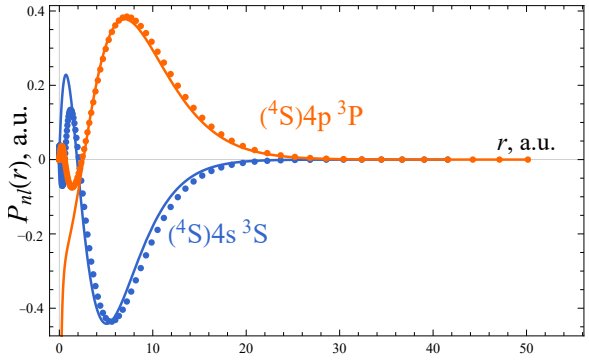
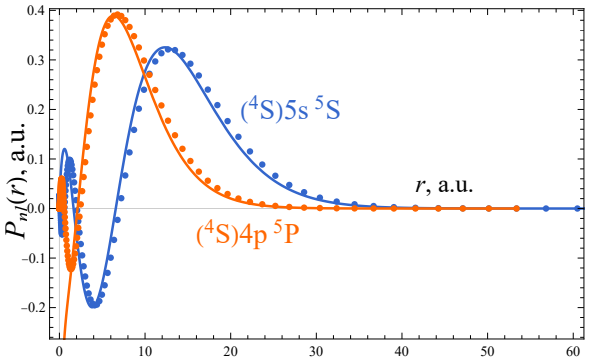


Figure 1. A part of the recorded spectra in 7000–11,000 cm^{-1} domain.



(**a**)



(**b**)

Figure 2. Radial electron wave functions of some S I $(^4S)nl\ (^{2S+1})L$ terms: (**a**) $L = l = 0$, $n = 4$, $S = 1$ and $L = l = 1$, $n = 4$, $S = 1$ (triplet terms); (**b**) $L = l = 0$, $n = 5$, $S = 2$ and $L = l = 1$, $n = 4$, $S = 2$ (quintet terms). Lines—QDT (4); dots—ab initio Hartree–Fock calculation using Cowan's code.

Table 1. QDs μ_l, integer principal (n) and orbital (l) quantum numbers, and non-integer effective principal (ν_{nl}) and orbital (l_{eff}) quantum numbers of the levels appearing in Figures 1 and 2.

Term $(^4S)nl\ (^{2S+1}L)$	n	l	ν_{nl}	$\mu_l(\nu_{nl})$	n_r	l_{eff}
$(^4S)4s(^3S)$	4	0	1.972	2.028	1	−0.02835
$(^4S)4s(^5S)$	4	0	1.883	2.117	1	−0.1166
$(^4S)4p(^3P)$	4	1	2.425	1.575	0	1.425
$(^4S)4p(^5P)$	4	1	2.337	1.663	0	1.337
$(^4S)4d(^3D)$	4	2	3.799	0.2014	1	1.799
$(^4S)4d(^5D)$	4	2	3.575	0.4247	1	1.575
$(^4S)5s(^3S)$	5	0	2.998	2.002	2	−0.001832
$(^4S)5s(^5S)$	5	0	2.922	2.078	2	−0.07844
$(^4S)5p(^3P)$	5	1	3.437	1.563	1	1.437
$(^4S)5p(^5P)$	5	1	3.374	1.626	1	1.374
$(^4S)6s(^3S)$	6	0	4.006	1.994	3	0.005860
$(^4S)6s(^5S)$	6	0	3.933	2.067	3	−0.06727
$(^4S)6p(^3P)$	6	1	4.403	1.597	2	1.403
$(^4S)6p(^5P)$	6	1	4.386	1.614	2	1.386

The QDT-calculated wave functions in Figure 2 are in satisfactory agreement with the ab initio wave functions because we took into account the dependence of QDs $\mu(E)$ on energy in a wide range, not only in near-threshold region $E \to -0$, as well as the function Ξ (5) in the normalization. This means that the nl-level wave function is not constructed from the experimental energy of *one* nl-level but includes information about *the entire l-series* (several values of n). We interpret this as some account of the multi-particle effects that distinguish the low excited states from the highly excited (Rydberg) ones. In high Rydberg states, the optical electron interacts quite weakly with the core electrons, whereas the low excited optical electron's wave functions overlap essentially with the core electron wave functions.

Note that the radius of the core r_c may be different for states with different orbital quantum numbers l, e.g., because of the centrifugal contribution $l(l+1)/2r^2$ to the intra-core potential. It follows from Table 1 that the radial $4p$ functions should have no nodes outside the core; therefore, we can estimate $r_c \simeq 2.5$ a. u. for p-electrons. Note that QDT wave functions demonstrate non-physical behavior inside the core because of the singularity of the Whittaker function at $r \to 0$. However, the radial integral (9) is affected only insignificantly by this small domain ($0 < r \lesssim r_c$) inside the core. Indeed, this integral contains the core-polarization correction

$$\kappa(r, r_c) = \frac{\alpha\, r}{(r^2 + r_c^2)^2}, \tag{2}$$

where α is the static dipole polarizability of the core. This correction accounts for some multi-particle effects that are due to the polarization of the atomic core [33–36]. At the $r \to 0$ limit, $\kappa(r, r_c)$ tends to zero, which reduces (together with the r factor) the contribution of the core domain ($0 < r \lesssim r_c$) into the radial integral (9). For large $r \gg r_c$, the polarization correction $\kappa(r, r_c) \sim \alpha/r^3$ vanishes as well so that $r(1 - \kappa(r, r_c)) \sim r$, and therefore, it is the large r domain that forms the main contribution to the integral (9). This is clearly seen for high-n Rydberg levels, for which the mean electron radius is of the order of $\sim n^2$. Given this fact, it is clear why both the QDT and the model potential theory give similar results for the matrix elements between high Rydberg states [31,32]. What is nontrivial is the fact that QDT, considered previously to be applicable for high n levels only, describes quantitatively even the wave functions of levels with low $n \gtrsim 4$ and even for the lowest of the $(^4S)nl$

terms (i.e., for $n = 4$ and $s = 0$); hence, the same can be expected for the transition matrix elements (9).

We compare the transition probabilities (A-values) between levels of $(^4S)nl$ terms (total 135) taken from the NIST Atomic Spectra Database [28] with our QDT-calculated A-values (see Formulas (7)–(9)). The comparison results are shown in Figure 3, from which it can be seen that most of the A-values calculated using QDT differ by no more than 12% from the values listed in the NIST ASD. The A-values compared in Figure 3 range from $\sim 5 \times 10^4$ to $\sim 2 \times 10^7$, which correspond to relatively strong transitions. For weaker transitions, the difference from the NIST is somewhat greater; some examples are given in Table 2.

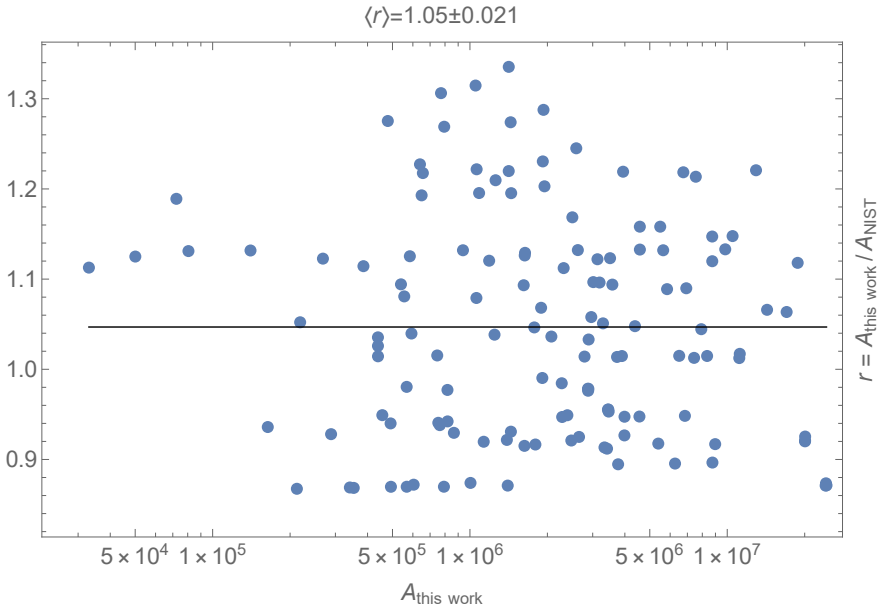


Figure 3. Comparison of the transition probabilities (A-values) calculated with QDT according to Equations (7)–(9) with the A-values given in the NIST ASD.

Table 2. Comparison of QDT-calculated probabilities for some weak transitions with the corresponding NIST values.

Wavenumber σ (cm^{-1})	Lower Level a	Upper Level b	$A_{b\leftarrow a}$ (s^{-1})	
			This Work	NIST
3567.46	$(^4S)5d(^5D_4)$	$(^4S)8f(^5F_4)$	1.12×10^4	1.28×10^4
3567.46	$(^4S)5d(^5D_4)$	$(^4S)8f(^5F_3)$	9.59×10^2	1.10×10^3
3567.12	$(^4S)5d(^5D_3)$	$(^4S)8f(^5F_3)$	2.01×10^4	2.31×10^4
3567.12	$(^4S)5d(^5D_3)$	$(^4S)8f(^5F_2)$	2.68×10^3	3.07×10^3
3566.79	$(^4S)5d(^5D_2)$	$(^4S)8f(^5F_1)$	4.47×10^3	5.13×10^3
3566.79	$(^4S)5d(^5D_2)$	$(^4S)8f(^5F_2)$	2.68×10^4	3.08×10^4
3527.40	$(^4S)4f(^3F_2)$	$(^4S)6d(^3D_2)$	1.24×10^4	1.12×10^4
3525.89	$(^4S)4f(^3F_3)$	$(^4S)6d(^3D_3)$	8.95×10^3	8.00×10^3
3525.87	$(^4S)4f(^3F_2)$	$(^4S)6d(^3D_3)$	2.56×10^2	2.29×10^2

Another way to test the capabilities of the modified QDT for calculating the radial wave functions of electrons is to compare the transition probabilities with experimental results. The simplest (albeit indirect) way to check these values experimentally is to construct Boltzmann plots, which are valuable tools in spectral diagnostics of plasmas.

For a line corresponding to emission the upper state $|b\rangle$ to the lower state $|a\rangle$, its intensity $I^{\text{calc}}_{b\to a}$ is proportional to the transition probability $A_{b\leftarrow a}$ (in optically thin LTE plasma characterized by electron temperature T):

$$I^{\text{calc}}_{b\to a} \sim g_b A_{b\leftarrow a} \sigma_{ab} \mathrm{e}^{-E_b/T}, \tag{3}$$

where E_b and g_b are the upper level's excitation energy and statistical weight, respectively, and the transition wavenumber is $\sigma_{ab} = \frac{1}{2\pi\hbar}(E_b - E_a)$.

Using the measured intensities, $I^{\text{obs}}_{b\to a}$, and the calculated ones, $I^{\text{calc}}_{b\to a}$ (3), we plotted the so-called Boltzmann plot, i.e., the logarithm of the $I^{\text{obs}}/I^{\text{calc}}$ ratio as a function of the upper level energy E_b. After fitting these data to the linear relationship of const $-\frac{E_b}{T}$, the effective plasma temperature can be estimated together with the so-called instrumental correction function $H(\sigma)$. The latter accounts for the spectral dependence of the recorded signal. Both the instrumental H function and temperature T are computed simultaneously with the iterating procedure described in Ref. [37].

Figure 4 shows a Boltzmann plot constructed on the base of our measured spectra. As can be seen from this figure, the points on the Boltzmann plot show a reasonable scatter from the approximating straight line, and the electronic temperature can be extracted from this plot with satisfactory (about 14%) accuracy. In the course of building the plot in Figure 4, we also calculated the instrumental correction function $H(\sigma) = \mathrm{e}^{-0.005447+0.00005015\sigma}$ in the $790 < \sigma < 11,000$ cm^{-1} spectral domain, where this function varies monotonically from 1.4 to 1.7, which corresponds to the minimal correction introduced to the experimental points. This fact is additional evidence in favor of the fact that QDT gives a satisfactory approximation for calculating the intensities of the lines measured in experimental spectra. The error bars in Figure 4 show the uncertainties (on the level of one standard deviation) of the $\log\left(I^{\text{obs}}/I^{\text{calc}}\right)$ values. These uncertainties were calculated by adding in quadrature of (i) uncertainty of QDT-calculated A-values (which was estimated as 14%) and (ii) uncertainty of the measured I^{obs} values. The latter arises because of the uncertainty of fitting the measured spectral peaks to a Lorentzian or Gaussian profile.

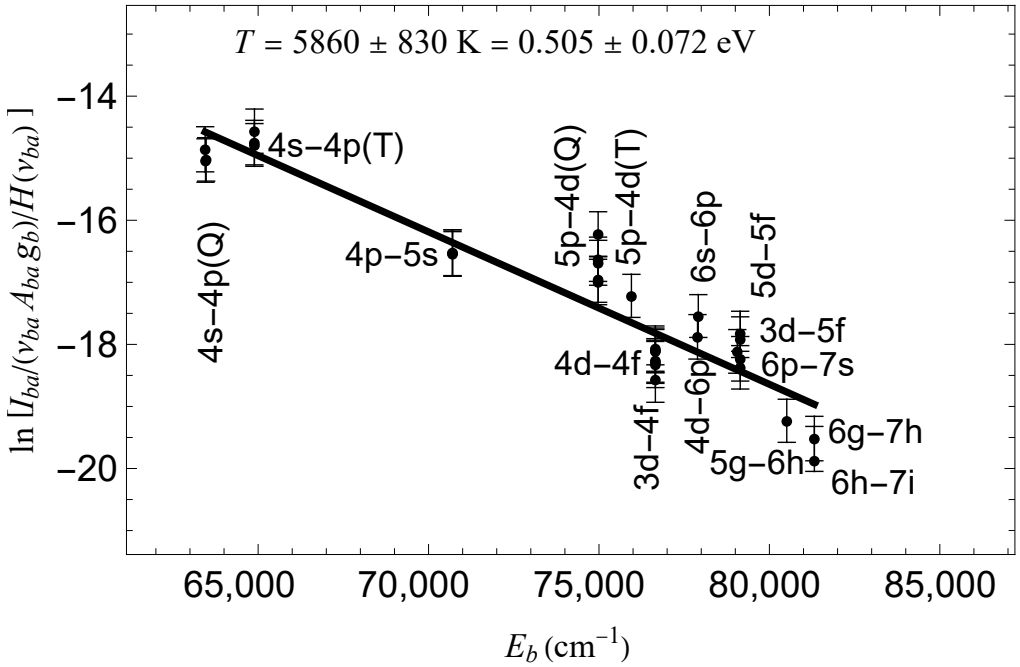


Figure 4. A Boltzmann plot constructed on the basis of our measured spectra. Q and T denote the quintet and triplet transitions, respectively.

3. Methods

3.1. Theory

Knowing the exact analytic expression for the GF of an atom allows one to easily derive the wave functions of both continuum and bound electronic states. It also enables the calculation of the properties due to atom–field interactions [38–40]. In QDT approximation, the analytical formulae for the electron radial wave functions were first derived using the QDT-GF [23] technique through hypergeometric functions, utilizing a relationship between the continuum states' scattering phases and the bound states' QDs [24,41]. The above-mentioned radial electron wave functions are constructed by calculating residues of the QDT-GF in its poles (which are determined by experimental spectroscopic data). The QDT-GF technique allows the calculation of two-photon matrix elements: frequency-dependent polarizability of alkali metal atoms [24] and the molecular hydrogen ion (see Ref. [42], where the two-photon ionization of H_2^+ was also calculated). For single-photon transitions involving very high atomic and molecular Rydberg states, a WKB–QDT was developed in Refs. [43,44].

All the above calculations are performed for systems with a single electron outside the filled shells. Ref. [45] proposed a modification of QDT-GF, called reduced-added GF (RAGF). The RAGF technique essentially uses the QD dependence on the electron energy, $\mu_l(E)$. It means that the QDs, μ_l, are to be determined not from the experimental energy of one level with a given l but rather from experimental energies of *the entire l-series*.

RAGF was used in Ref. [45] to calculate two-photon transitions (namely dynamical polarizabilities) of many atoms having several valence (including Rydberg) electrons outside the filled shells. In this paper, we use the results of the RAGF technique to calculate the single-photon transition probabilities in atomic sulfur S I. Specifically, we use an analytical expression [45] for the radial wave functions in terms of Whittaker functions [46]:

$$P_{nl}(r) = \frac{Z^{1/2}}{\nu_{nl}} W_{\nu_{nl},l+1/2}\left(\frac{2Zr}{\nu_{nl}}\right)\left[\frac{\Xi_l(E_{nl})}{\Pi_l(\nu_{nl})\Gamma(l+1+\nu_{nl})\Gamma(\nu_{nl}-l)\left(1+\frac{\partial\mu_l(\nu_{nl})}{\partial\nu}\right)}\right]^{1/2}. \quad (4)$$

The normalization factor in Equation (4) is different from that traditionally appearing in QDT wave functions [10]. This factor contains an entire analytic function of energy, $\Xi(E)$, which can be fully determined by its values on a countable set of points, as an approximation to which we can take the experimental spectrum points, E_{nl}:

$$\Xi_l(E_{nl}) = \Pi_l(n), \quad n \geq l+1, \quad (5)$$

$$\Pi_l(\nu) = \frac{\nu^{2l}}{\prod_{k=0}^{l-1}(k+\mu_l+\nu)(k+1-\mu_l-\nu)}. \quad (6)$$

The RAGF theory introduces Ξ and Π functions to eliminate "waste" pure-Coulombic QDT-GF poles; such poles arise if the QD μ_l is obtained from only one experimental energy E_{nl} of a high-n level. However, this is a satisfactory approximation for highly excited Rydberg levels only, i.e., in the limit $n \to \infty$ or, what is the same, $E \to -0$. In fact, the functions (5) and (6) bring an additional energy dependence into the radial wave function (4) together with the derivative $\partial\mu_l(\nu)/\partial\nu$ of the quantum defect μ_l ($E = -1/2\nu^2$) over a wide energy range (not just near the $E \to -0$ threshold). The practical calculation of this derivative is performed with the help of fitting of $\mu_l(E)$ from a discrete set of its values, $\mu_l(E_{nl})$, at the experimental levels of l-series. The fitting can be performed, for example, according to Ritz expansion; see [47] (Equation (12)) or [48] (Equations (10.10) and (11.52)). Obviously,

one needs as many experimental energies in a Rydberg l-series as possible to provide a reasonable accuracy of the $\partial\mu_l(\nu)/\partial\nu$ calculation procedure.

The probability $A_{b\leftarrow a}$ of radiative transition from the upper $|a\rangle$ state to the lower $|b\rangle$ state is expressed through the line strength $S_{a\to b}$ or oscillator strength $f_{a\to b}$ [47,49]:

$$\begin{aligned} S_{a\to b} &= \sum_{M_a,M_b} |\langle\gamma_a J_a M_a|\mathcal{D}|\gamma_b J_b M_b\rangle|^2, \\ -f_{a\to b} &= \frac{2m}{3\hbar e^2}\frac{\omega}{g_a} S_{a\to b}, \\ A_{b\leftarrow a} &= \frac{4\omega^3}{3\hbar c^3}\frac{1}{g_b} S_{a\to b} = \frac{2\omega^2 e^2}{mc^3}|f_{a\to b}|, \end{aligned} \tag{7}$$

where $\omega = \omega_{a\to b} = (E_a - E_b)/\hbar$ is the transition frequency and $g_{b,a} = [J_{b,a}] := 2J_{b,a} + 1$ are the statistical weights of the corresponding levels. The line strength $S_{a\to b}$ is the square of the dipole transition matrix element summed by projections $M_{a,b}$ of the total orbital moments $J_{a,b}$ of the initial and final term. The additional quantum numbers, $\gamma_{a,b}$, are determined, for example, by the momentum coupling scheme. For the LS coupling scheme, which is applicable to the neutral sulfur states, $\gamma_{a,b}$ include the total orbital momentum $L_{a,b}$ and spin $S_{a,b}$ of the initial and final terms, and the line strength can be expressed through the $6j$-symbols using the angular momentum [49] technique:

$$\begin{aligned} S_{a\to b} &= \sum_{M_a,M_b} |\langle S_a L_a J_a M_a|\mathcal{D}|S_b L_b J_b M_b\rangle|^2 \\ &= [J_a]\,[J_b]\,[L_a]\,[L_b] \begin{Bmatrix} L_a & J_a & S_a \\ J_b & L_b & 1 \end{Bmatrix}^2 \begin{Bmatrix} l_a & L_a & L_a^{\mathrm{c}} \\ L_b & l_b & 1 \end{Bmatrix}^2 |\langle n_a l_a\|\mathcal{D}\|n_b l_b\rangle|^2, \end{aligned} \tag{8}$$

where L^{c} is the core orbital momentum. Most of the terms that form prominent lines in our S I spectra are characterized by the $3s^2\,3p^3\,{}^4S$ core term, i.e., $L^{\mathrm{c}} = 0$; in this paper, we restrict ourselves to terms with the $3s^2\,3p^3({}^4S)$ core.

The following radial integral gives the reduced dipole matrix element (8) (where e is the electron charge):

$$\langle n_a l_a\|\mathcal{D}\|n_b l_b\rangle = e\,\max\{l_a, l_b\}\int_{r_{\mathrm{c}}}^{\infty} r(1-\kappa(r,r_{\mathrm{c}}))P_{n_a l_a}(r)P_{n_b l_b}(r)\,\mathrm{d}r, \tag{9}$$

where $\kappa(r, r_{\mathrm{c}})$ accounts for (multi-particle) core polarization effects (see Equation (2) and the discussion in Section 2).

3.2. Experiment

A microwave discharge in a buffer gas of helium was used to generate sulfur emission lines. The measurements were carried out in a quartz tube equipped with windows (KBr and CaF_2) at its ends. This allowed us to obtain spectra in two spectral domains: 760–4000 cm^{-1} and 2000–6500 cm^{-1}. Two detectors, HgCdTe (MCT) and InSb, were used for these domains, respectively. Each detector had a different sensitivity and was cooled by liquid nitrogen. To cover the spectral range from 2000 cm^{-1} to 7000 cm^{-1}, we used several Northumbria Optical Coatings Ltd. (Boldon, UK) bandpass interference filters. The spectral regions with wavelength numbers below 2000 cm^{-1} and above 7000 cm^{-1} were measured without interference filters.

We conducted a plasma discharge in a 99.996 % helium stream at a pressure of 93–200 Pa (0.7–1.5 Torr). For a microwave source, we used a Microtron 200 W instrument operating at 2.5 GHz and 70 W power. At the start of the microwave discharge, it was necessary to optimize the helium pressure to ensure easy ignition and stabilize the

microwave power at the optimum level. Sulfur powder with a purity of 99.99% was used as a sample. During the measurement, the discharge conditions varied in space and time as the sulfur diffused into the colder edges. It was observed that the plasma spectra show traces of impurities, such as O, N, and Ar, in the discharge.

The Fourier transfer spectroscopy (FTS) was performed on a Bruker IFS 120 spectrometer (Bruker Corporation, Leipzig, Germany). The spectral resolution was 0.04 cm^{-1} in the 790–2000 cm^{-1} domain and 0.05 cm^{-1} in the 2000–110,000 cm^{-1} domain. During prolonged measurements in the He plasma discharge, the windows were covered with sulfur layers, resulting in a decrease in the intensity of the signal. Several series of S I spectra recordings were performed to maintain stable results, and in each case, the sulfur samples were replaced together with the KBr and CaF_2 optical windows. To increase SNR, the spectrometer performed about a hundred scans.

Water absorption lines were used to calibrate the measured spectra; we took the high-precision wavenumbers of these lines from HITRAN [50]. For a more detailed description of the calibration, as well as the time-resolved FTS, see Refs. [51,52].

4. Concluding Remarks

QDT (quantum defect theory) is a semi-phenomenological theory that is successfully used for analytic calculations of a number of data needed in astrophysics, low-temperature plasma, and other applications of atomic and molecular physics, such as radiative transition probabilities, polarizabilities, photoionization cross-sections, etc. It was believed that QDT is applicable only for highly excited (Rydberg) electrons in a field of a closed-shell atomic core that essentially takes place in atoms with hydrogen-like spectrum (such as alkali metal atoms).

In the present paper, we use a modification of QDT that allows us to calculate transition probabilities for an atom with a more complex spectrum, sulfur S I. This modification is due to taking into account the energy dependence of quantum defects. We show that the modified QDT provides a good description for radial wave functions even of low excited S I terms as well as for radiation transitions involving such terms (not only the high-Rydberg terms).

Note that in QDT, because of its semi-phenomenological nature, the level energies (and, therefore, the line wavelengths) are not calculated, but rather they are considered as external input parameters from which the quantum defects $\mu(E)$ are calculated. In turn, once $\mu(E)$ are known, the radial electron wave functions can be calculated according to Equations (4) and (7). Using these wave functions, the transition probabilities (8) are calculated through the squares of one-photon matrix elements (9).

To check our QDT calculation of dipole transition probabilities (A-values), we took 135 relatively strong ($5 \times 10^4 \lesssim A \lesssim 2 \times 10^7$) transitions between levels of $(^4S)nl$ terms from the NIST Atomic Spectra Database [28]; see Figure 3. This list includes transitions $(^4\mathrm{S})n_1\mathrm{s}$–$(^4\mathrm{S})n_2\mathrm{p}$ with $n_1 = 4, 5$ and $n_2 = 4$–7; $(^4S)4p$–$(^4S)n_2s$ with $n_2 = 5$–9; $(^4S)4p$–$(^4S)n_2d$ with $n_2 = 3$–8; $(^4S)3d$–$(^4S)n_2f$ with $n_2 = 4$–9. Most of these A-values calculated using QDT differ by no more than 12% from the values listed in the NIST ASD. For weaker transitions, the difference from the NIST is about 15%; some examples are given in Table 2 for quintet $(^4\mathrm{S})5\mathrm{d}$–$(^4\mathrm{S})8\mathrm{f}$ transitions and triplet–quintet $(^4\mathrm{S})4\mathrm{f}$–$(^4\mathrm{S})6\mathrm{d}$ transitions.

We also made a comparison of QDT-calculated A-values with experimental results. High-resolution Fourier transfer spectroscopy was used to record S I spectra in the infrared domain from 790 to 11,000 cm^{-1} in a gas discharge plasma. By making Boltzmann plots for these spectra, we show that QDT gives reasonable estimates for the intensities of the spectral peaks in our experimental spectra.

Author Contributions: Conceptualization, S.C. and N.L.M.; methodology, M.F.; software, P.K. and E.M.Z.; formal analysis, A.V.M.; data curation, O.V.Z.; visualization, A.V.N.; writing—original draft preparation, V.E.C.; writing—review and editing, N.L.M. All authors have read and agreed to the published version of the manuscript.

Funding: This research was funded by Ministry of Education and Science of the Russian Federation Project No. FZGU-2023-0007.

Data Availability Statement: The data are available from the authors.

Conflicts of Interest: The authors declare no conflict of interest.

Abbreviations

FTS	Fourier transform spectroscopy
GF	Green's function
IP	Ionization potential
IR	Infrared
LTE	Local thermodynamic equilibrium
QD	Quantum defect (see (1))
QDT	Quantum defect theory
RAGF	Reduced-added Green's function (see [45])
SNR	Signal-to-noise ratio

References

1. Maillard, J.P. Infrared astronomy beyond JWST: The Moon perspective. *Phil. Trans. R. Soc. A* **2024**, *382*, 20230070. [CrossRef] [PubMed]
2. Pickering, J.; Blackwell-Whitehead, R.; Thorne, A.; Ruffoni, M.; Holmes, C. Laboratory measurements of oscillator strengths and their astrophysical applications. *Can. J. Phys.* **2011**, *89*, 387–393. [CrossRef]
3. Bhatia, A.K. Scattering and Its Applications to Various Atomic Processes: Elastic Scattering, Resonances, Photoabsorption, Rydberg States, and Opacity of the Atmosphere of the Sun and Stellar Objects. *Atoms* **2020**, *8*, 78. [CrossRef]
4. Srećković, V.A.; Ignjatović, L.M.; Dimitrijević, M.S. Symmetric Atom–Atom and Ion–Atom Processes in Stellar Atmospheres. *Atoms* **2018**, *6*, 1. [CrossRef]
5. Hillier, D.J. Photoionization and Electron–Ion Recombination in Astrophysical Plasmas. *Atoms* **2023**, *11*, 54. [CrossRef]
6. Nave, G.; Nahar, S.; Zhao, G. Division B Commission 14 Working Group: Atomic Data. *Trans. IAU* **2015**, *11*, 103–119. [CrossRef]
7. Dimitrijević, M.S.; Sahal-Bréchot, S. On the Application of Stark Broadening Data Determined with a Semiclassical Perturbation Approach. *Atoms* **2014**, *2*, 357–377. [CrossRef]
8. Alexiou, S. Effects of Spiralling Trajectories on White Dwarf Spectra: High Rydberg States. *Atoms* **2023**, *11*, 141. [CrossRef]
9. Papoulia, A.; Ekman, J.; Gaigalas, G.; Godefroid, M.; Gustafsson, S.; Hartman, H.; Li, W.; Radžiūtė, L.; Rynkun, P.; Schiffmann, S.; et al. Coulomb (Velocity) Gauge Recommended in Multiconfiguration Calculations of Transition Data Involving Rydberg Series. *Atoms* **2019**, *7*, 106. [CrossRef]
10. Seaton, M.J. Quantum defect theory. *Rep. Prog. Phys.* **1983**, *46*, 167–257. [CrossRef]
11. Letunov, A.Y.; Lisitsa, V.S. Review of Rydberg Spectral Line Formation in Plasmas. *Atoms* **2023**, *11*, 133. [CrossRef]
12. Lee, C.W. Inter-Series Interactions on the Atomic Photoionization Spectra Studied by the Phase-Shifted Multichannel-Quantum Defect Theory. *Atoms* **2017**, *5*, 21. [CrossRef]
13. Baig, M.A. Measurement of Photoionization Cross-Section for the Excited States of Atoms: A Review. *Atoms* **2022**, *10*, 39. [CrossRef]
14. Gning, M.T.; Sakho, I. Photoionization Study of Neutral Chlorine Atom. *Atoms* **2023**, *11*, 152. [CrossRef]
15. Khuskivadze, A.A.; Chibisov, M.I.; Fabrikant, I.I. Adiabatic energy levels and electric dipole moments of Rydberg states of Rb_2 and Cs_2 dimers. *Phys. Rev. A* **2002**, *66*, 042709. [CrossRef]
16. Narits, A.; Kislov, K.; Lebedev, V. Electron-Impact Excitation and Dissociation of Heavy Rare Gas Heteronuclear Ions via Transitions to Charge Transfer States. *Atoms* **2023**, *11*, 60. [CrossRef]
17. Pazyuk, E.; Revina, E.; Stolyarov, A. Ab Initio Long-Range Stud. Electron. Transit. Dipole Moments Low-Lying States Rb_2 Cs_2 Mol. *J. Quant. Spectrosc. Radiat. Transf.* **2016**, *177*, 283–290. [CrossRef]
18. Li, H.; Li, M.; Makrides, C.; Petrov, A.; Kotochigova, S. Universal Scattering of Ultracold Atoms and Molecules in Optical Potentials. *Atoms* **2019**, *7*, 36. [CrossRef]

19. Dimitrijević, M.S.; Srećković, V.A.; Zalam, A.A.; Bezuglov, N.N.; Klyucharev, A.N. Dynamic Instability of Rydberg Atomic Complexes. *Atoms* **2019**, *7*, 22. [CrossRef]
20. Simons, G. New procedure for generating valence and Rydberg orbitals. I. Atomic oscillator strengths. *J. Chem. Phys.* **1974**, *60*, 645–649. [CrossRef]
21. Manakov, N.L.; Ovsiannikov, V.D.; Rapoport, L.P. Atoms in a laser field. *Phys. Rep.* **1986**, *141*, 320–433. [CrossRef]
22. Il'inova, E.Y.; Ovsyannikov, V.D. Modified Fues potential for many-electron atoms. *Opt. Spectrosc.* **2008**, *105*, 647–656. [CrossRef]
23. Zon, B.A.; Manakov, N.L.; Rapoport, L.P. Semiphenomenological Green's Function of the Optical Electron in a Complex Atom. *Sov. Phys. Dokl.* **1970**, *14*, 904.
24. Chernov, V.; Manakov, N.; Starace, A. Exact analytic relation between quantum defects and scattering phases with applications to Green's functions in quantum defect theory. *Eur. Phys. J. D* **2000**, *8*, 347–359. [CrossRef]
25. Walsh, C. *The Chemical Biology of Sulfur*; Royal Society of Chemistry: London, UK, 2020. [CrossRef]
26. Turrini, D.; Schisano, E.; Fonte, S.; Molinari, S.; Politi, R.; Fedele, D.; Panic, O.; Kama, M.; Changeat, Q.; Tinetti, G. Tracing the Formation History of Giant Planets in Protoplanetary Disks with Carbon, Oxygen, Nitrogen, and Sulfur. *Astrophys. J.* **2021**, *909*, 40. [CrossRef]
27. Bernard-Salas, J.; Pottasch, S.R.; Gutenkunst, S.; Morris, P.W.; Houck, J.R. Neon and Sulfur Abundances of Planetary Nebulae in the Magellanic Clouds. *Astrophys. J.* **2008**, *672*, 274. [CrossRef]
28. Kramida, A.; Ralchenko, Y.; Reader, J.; NIST ASD Team. *NIST Atomic Spectra Database,* version 5.10; NIST: Gaithersburg, MD, USA, 2022. [CrossRef]
29. Cowan, R.D. *The Theory of Atomic Structure and Spectra*; Los Alamos Series in Basic and Applied Sciences; University of California Press: Berkeley, CA, USA, 1981.
30. Kramida, A. Cowan Code: 50 Years of Growing Impact on Atomic Physics. *Atoms* **2019**, *7*, 64. [CrossRef]
31. Glukhov, I.L.; Mokhnenko, S.N.; Nikitina, E.A.; Ovsiannikov, V.D. Natural widths and blackbody radiation induced shift and broadening of Rydberg levels in magnesium ions. *Eur. Phys. J. D* **2015**, *69*, 1. [CrossRef]
32. Glukhov, I.L.; Kamenski, A.A.; Ovsiannikov, V.D.; Palchikov, V.G. Precision Spectroscopy of Radiation Transitions between Singlet Rydberg States of the Group IIb and Yb Atoms. *Photonics* **2023**, *10*, 1153. [CrossRef]
33. Veselov, M.G.; Shtoff, A.V. Calculation of oscillator strengths of principal series of lithium in adiabatic approximation. *Opt. Spectrosc.* **1969**, *26*, 177.
34. Beigman, I.L.; A., V.L.; Shevelko, V.P. Effect of polarization of atomic core on oscillator strengths and photoionization cross-sections of alkali element atoms. *Opt. Spectrosc.* **1970**, *28*, 229.
35. Chichkov, B.N.; Shevelko, V.P. Dipole Transitions in Atoms and Ions With One Valence Electron. *Phys. Scr.* **1981**, *23*, 1055–1065. [CrossRef]
36. Astapenko, V.A.; Bureeva, L.A.; Lisitsa, V.S. Polarization effects in atomic transitions. *Phys. Uspekhi* **2002**, *45*, 149–184. [CrossRef]
37. Kramida, A. Critical Evaluation of Data on Atomic Energy Levels, Wavelengths, and Transition Probabilities. *Fusion Sci. Technol.* **2013**, *63*, 313–323. [CrossRef]
38. Derevianko, A.; Ovsiannikov, V.D.; Pal'chikov, V.G.; Johnson, W.R.; Plante, D.R.; von Oppen, G. Higher-order Stark effect on an excited helium atom. *Phys. Rev. A* **1999**, *60*, 986–995. [CrossRef]
39. Romanov, A.A.; Silaev, A.A.; Vvedenskii, N.V.; Breev, I.V.; Flegel, A.V.; Frolov, M.V. Second-harmonic generation of a short XUV pulse interacting with an IR-laser-dressed atom. *Phys. Rev. A* **2022**, *106*, 063101. [CrossRef]
40. Romanov, A.A.; Silaev, A.A.; Sarantseva, T.S.; Flegel, A.V.; Vvedenskii, N.V.; Frolov, M.V. Channel separation of secondary generated radiation induced by orthogonal XUV and IR pulses. *Opt. Lett.* **2023**, *48*, 3583–3586. [CrossRef] [PubMed]
41. Norman, G.E. Basis for the Quantum Defect Method. *Opt. Spectrosc. (USSR)* **1962**, *12*, 183.
42. Davydkin, V.A.; Rapoport, L.P. The two-photon ionization of H_2^+. *J. Phys. B At. Mol. Opt. Phys.* **1974**, *7*, 1101–1108. [CrossRef]
43. Davydkin, V.A.; Zon, B.A. Radiation And Polarization Characteristics Of Rydberg Atomic States. Part I. *Opt. Spectrosc. (USSR)* **1981**, *51*, 13–150.
44. Alcheev, P.G.; Buenker, R.J.; Chernov, V.E.; Zon, B.A. Oscillator strengths for Rydberg states in ArH calculated in QDT approximation. *J. Mol. Spectrosc.* **2003**, *218*, 190–196. [CrossRef]
45. Chernov, V.E.; Dorofeev, D.L.; Kretinin, I.Y.; Zon, B.A. Method of the reduced-added Green function in the calculation of atomic polarizabilities. *Phys. Rev. A* **2005**, *71*, 022505. [CrossRef]
46. Bateman, H.; Erdélyi, A. *Higher Transcendental Functions*; McGraw-Hill: New York, NY, USA 1953.
47. Martin, W.; Wiese, W. *Atomic, Molecular, and Optical Physics Handbook (Version 2.2)*; Springer: New York, NY, USA, 2002.
48. Drake, G.W.F. (Ed.) *Springer Handbook of Atomic, Molecular, and Optical Physics*; Springer: New York, NY, USA, 2006.
49. Sobelman, I.I. *Atomic Spectra and Radiative Transitions*; Springer Series in Chemical Physics; Springer: Berlin/Heidelberg, Germany, 1979; Volume 1.
50. Gordon, I.; Rothman, L.; Hargreaves, R.; Hashemi, R.; Karlovets, E.; Skinner, F.; Conway, E.; Hill, C.; Kochanov, R.; Tan, Y.; et al. The HITRAN2020 molecular spectroscopic database. *J. Quant. Spectrosc. Radiat. Transf.* **2022**, *277*, 107949. [CrossRef]

51. Civiš, S.; Kubelík, P.; Ferus, M.; Chernov, V.E.; Zanozina, E.M.; Juha, L. Laser ablation of an indium target: Time-resolved Fourier-transform infrared spectra of In I in the 700–7700 cm^{-1} range. *J. Anal. At. Spectrom.* **2014**, *29*, 2275–2283. [CrossRef]
52. Civiš, S.; Ferus, M.; Chernov, V.E.; Zanozina, E.M.; Juha, L. Zn I spectra in the 1300–6500 cm^{-1} range. *J. Quant. Spectrosc. Radiat. Transf.* **2014**, *134*, 64–73. [CrossRef]

Disclaimer/Publisher's Note: The statements, opinions and data contained in all publications are solely those of the individual author(s) and contributor(s) and not of MDPI and/or the editor(s). MDPI and/or the editor(s) disclaim responsibility for any injury to people or property resulting from any ideas, methods, instructions or products referred to in the content.